Supporting Information

Effectively increased efficiency for electroreduction of carbon monoxide using supported polycrystalline copper powder electrocatalysts

Jing Li[1], Kuan Chang[1], Haochen Zhang[1], Ming He[1], William A. Goddard, III[2], Jingguang G. Chen[1,3], Mu-Jeng Cheng[4] & Qi Lu[1*]

[1]State Key Laboratory of Chemical Engineering, Department of Chemical Engineering, Tsinghua University, Beijing 100084, China.

[2]Materials and Process Simulation Center, California Institute of Technology, Pasadena, California 91125, United States.

[3]Department of Chemical Engineering, Columbia University, New York, New York 10027, United States.

[4]Department of Chemistry, National Cheng-Kung University, Tainan 701, Taiwan.

Jing Li and Kuan Chang contributed equally to this work.

*e-mail: luqicheme@mail.tsinghua.edu.cn

Figure S1. Image of the three-electrode H-cell employed for CO electrolysis study.

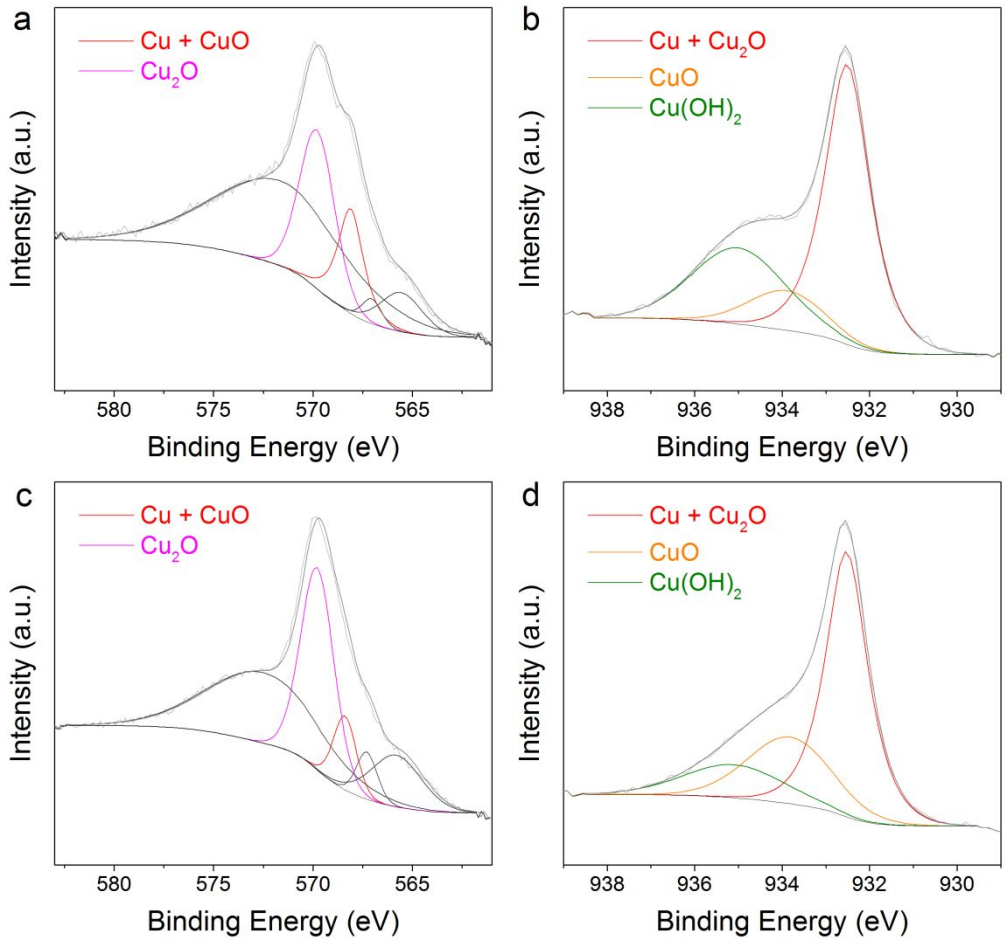

Figure S2. X-ray spectroscopy characterizations for both Cu powders. a, Dendritic Cu LMM spectrum. **b,** Dendritic Cu $2p_{3/2}$ spectrum. **c,** Spherical Cu LMM spectrum. **d,** Spherical Cu $2p_{3/2}$ spectrum. The three additional peaks (dark grey) in the Cu LMM spectra located at approximately 572.8, 567.0 and 565.1 eV only represent different transition states.[1-3]

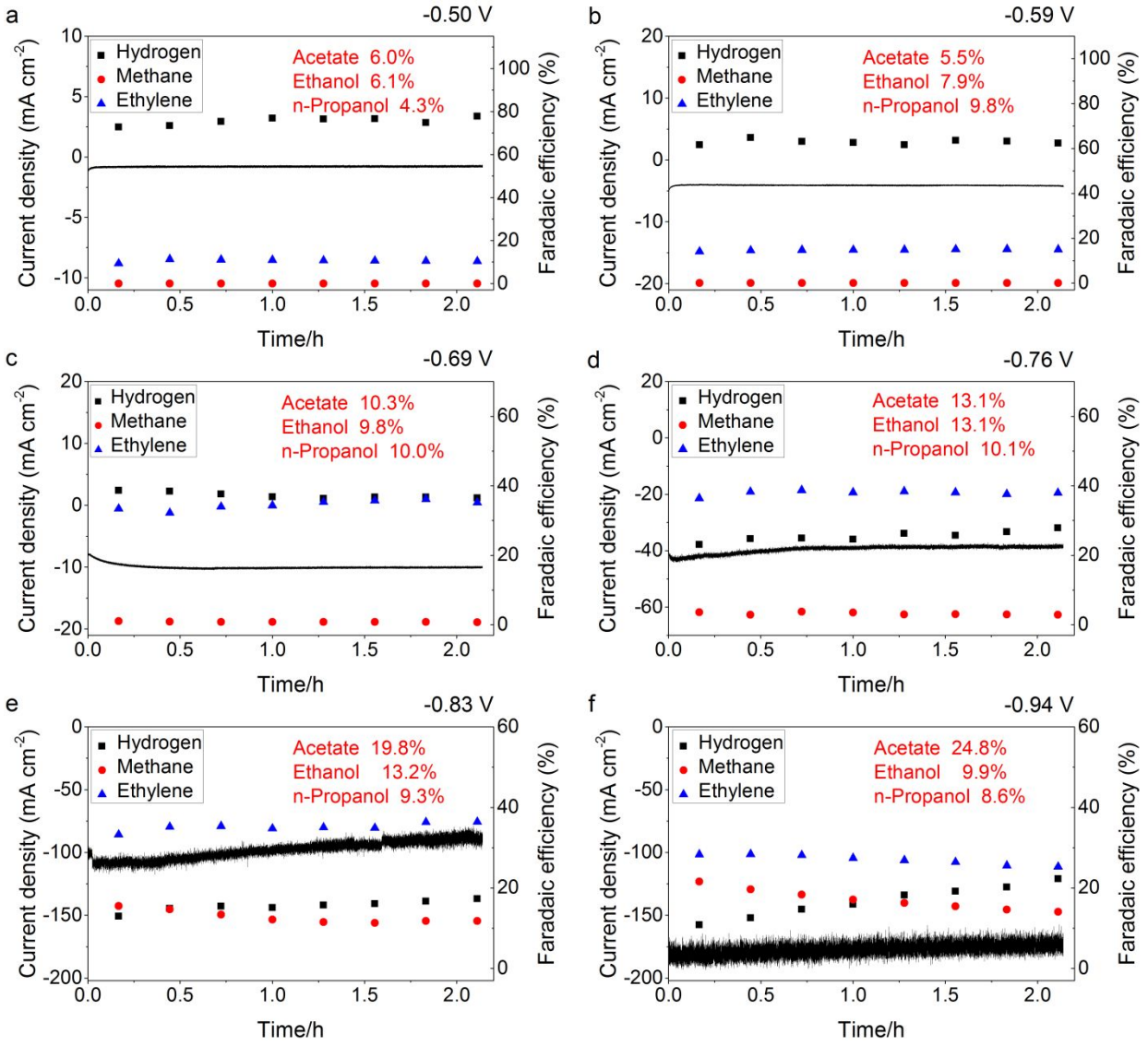

Figure S3. Electrolysis data for dendritic copper powder. Current density as a function of time for CO electroreduction at -0.5 V (a), -0.59 V (b), -0.69 V (c), -0.76 V (d), -0.83 V (e) and -0.94 V (f). The faradic efficiencies for hydrogen, methane and ethylene were calculated from each individual gas chromatograph spectrum. The efficiencies for acetate, ethanol and n-propanol were obtained at the end of the electrolysis.

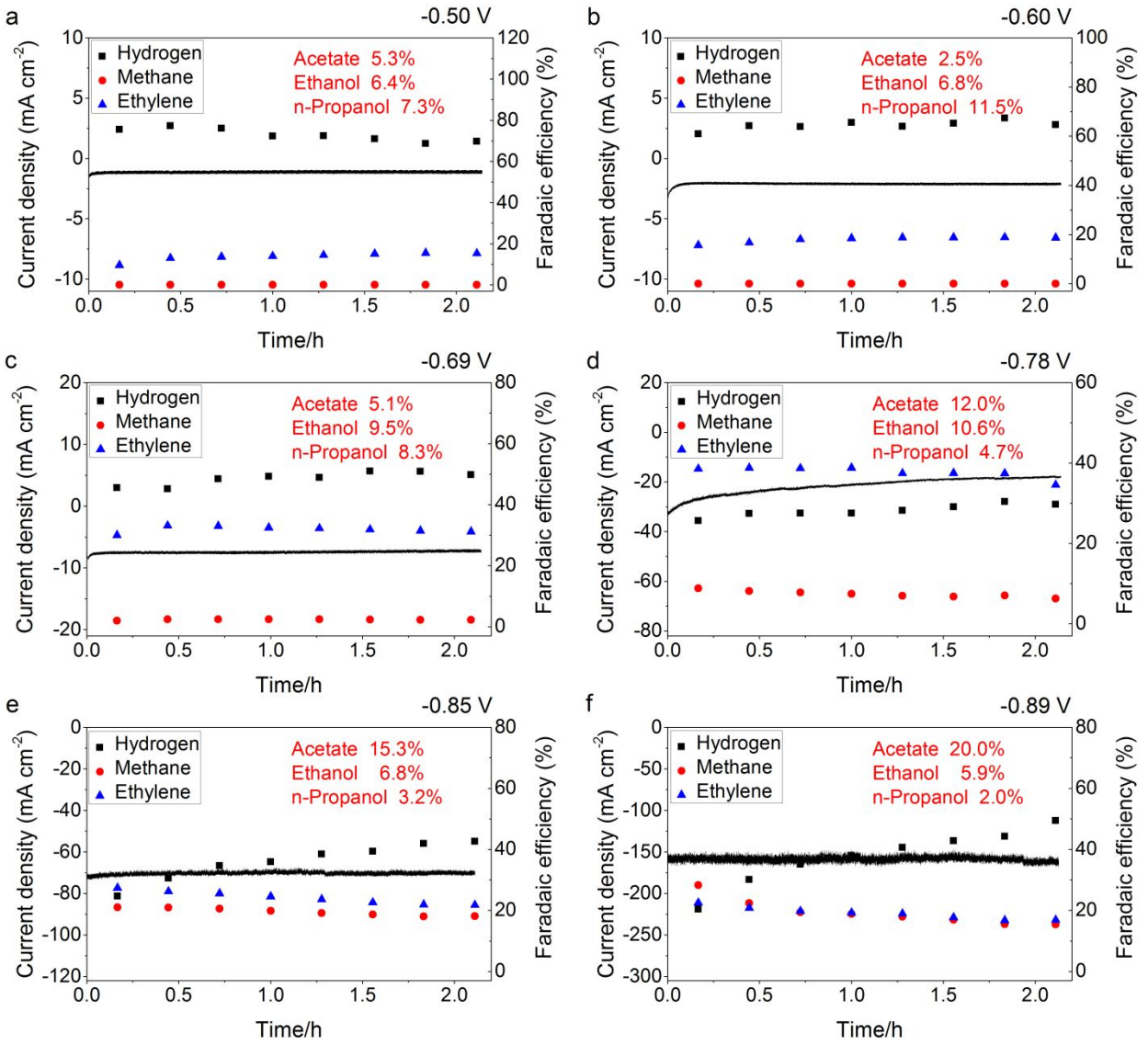

Figure S4. Electrolysis data for spherical copper powder. Current density as a function of time for CO electroreduction at -0.5 V (a), -0.60 V (b), -0.69 V (c), -0.78 V (d), -0.85 V (e) and -0.89 V (f). The faradic efficiencies for hydrogen, methane and ethylene were calculated from each individual gas chromatograph spectrum. The efficiencies for acetate, ethanol and n-propanol were obtained at the end of the electrolysis.

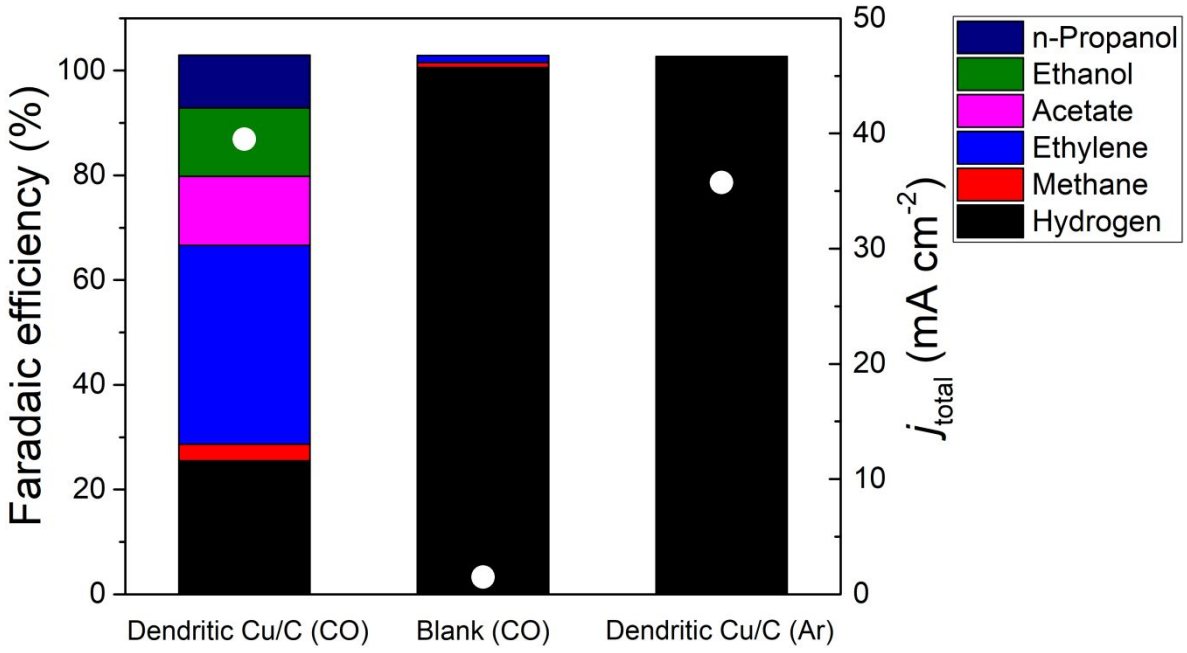

Figure S5. Controlled experiments. Electrolysis results for the dendritic Cu/C electrode and a blank carbon fiber paper electrode in an CO-purged electrolyte as well as the dendritic Cu/C electrode in an Ar-purged electrolyte compared at -0.76 V.

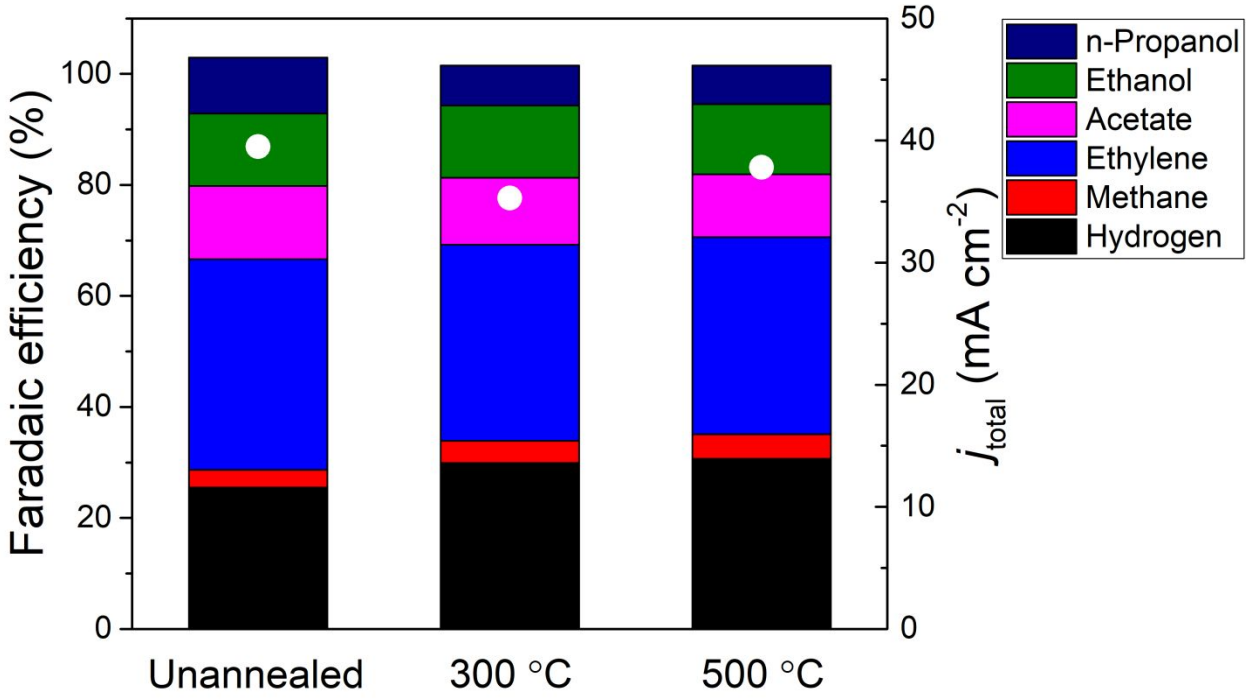

Figure S6. CO electrolysis results for annealed dendritic Cu powder. The dendritic Cu powder was annealed in 5% H_2 in Ar gas at 300 °C and 500 °C for two hours. No obvious CO electroreduction performance changes were observed compared to the unannealed Cu powder at -0.76 V.

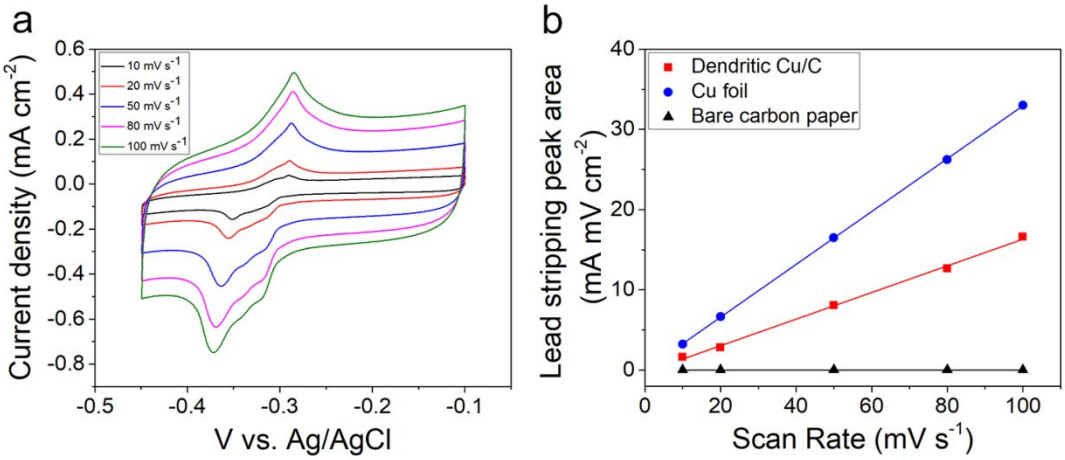

c

Electrode	Lead stripping charge (μC/cm^2)	Roughness factor
Cu foil	329.3	1.00
Dendritic Cu/C	165.9	0.50

Figure S7. ECSA measurement. (a) Cyclic voltammetry study of Pb UPD on a pristine dendritic Cu/C electrode at different scanning rates. (b) The measured lead stripping peak area vs. scanning rate for dendritic Cu/C electrode, an electrochemically polished Cu foil, and a bare carbon paper support. (c) The measured lead stripping charge and the corresponding roughness factor.

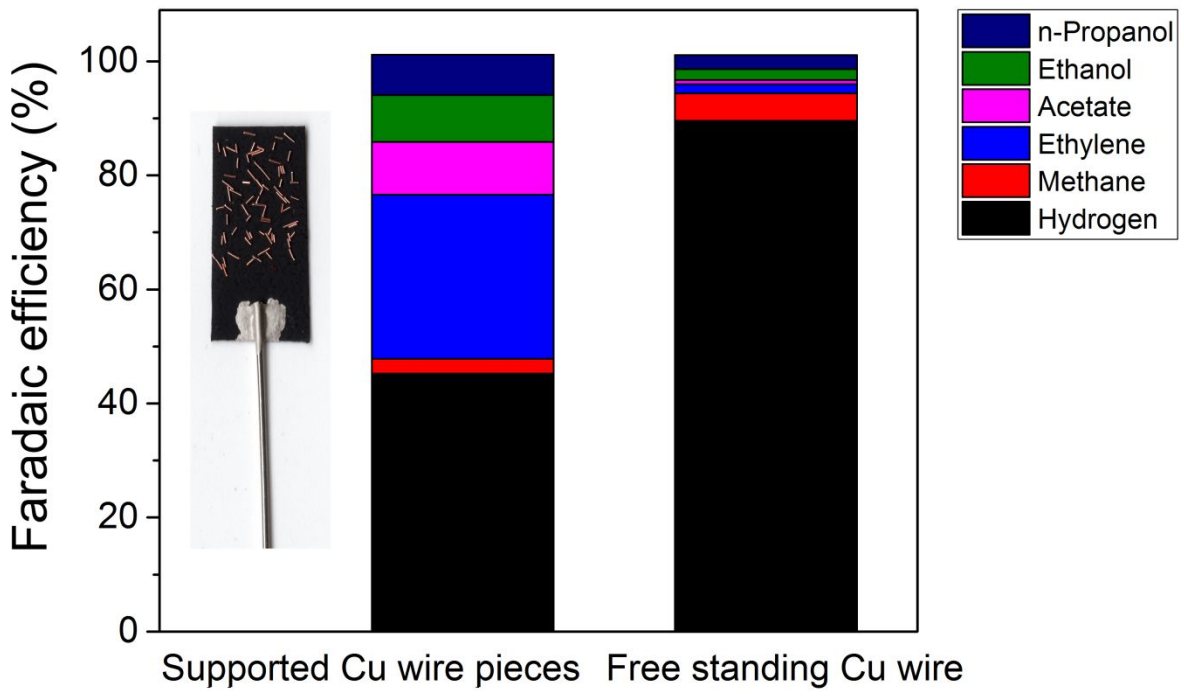

Figure S8. CO electrolysis results for free-standing Cu wire and supported Cu wire pieces at -0.9 V. Inset, photo of the electrode fabricated using Cu wire pieces supported on carbon fiber paper.

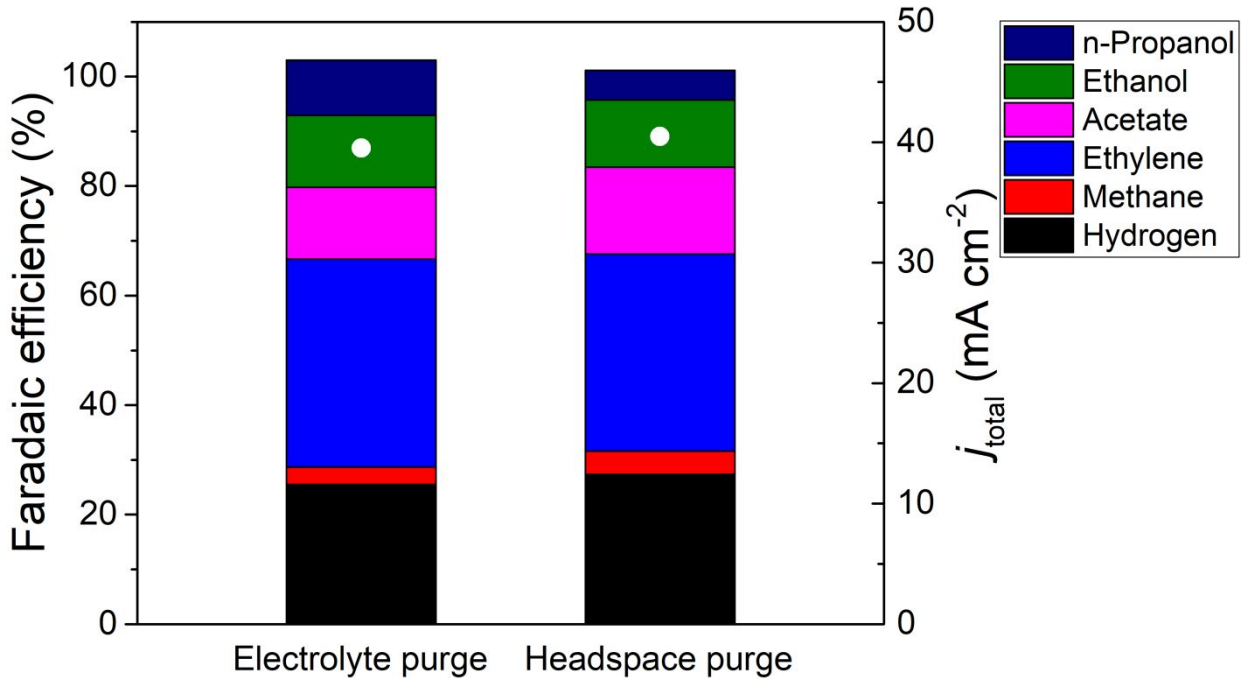

Figure S9. CO electrolysis results of dendritic Cu/C electrodes at -0.76 V when electrolyte was purged and only headspace was purged. This result indicates that the CO transported to the reaction sites is not from the direct contact of the gas stream purged into the electrolyte.

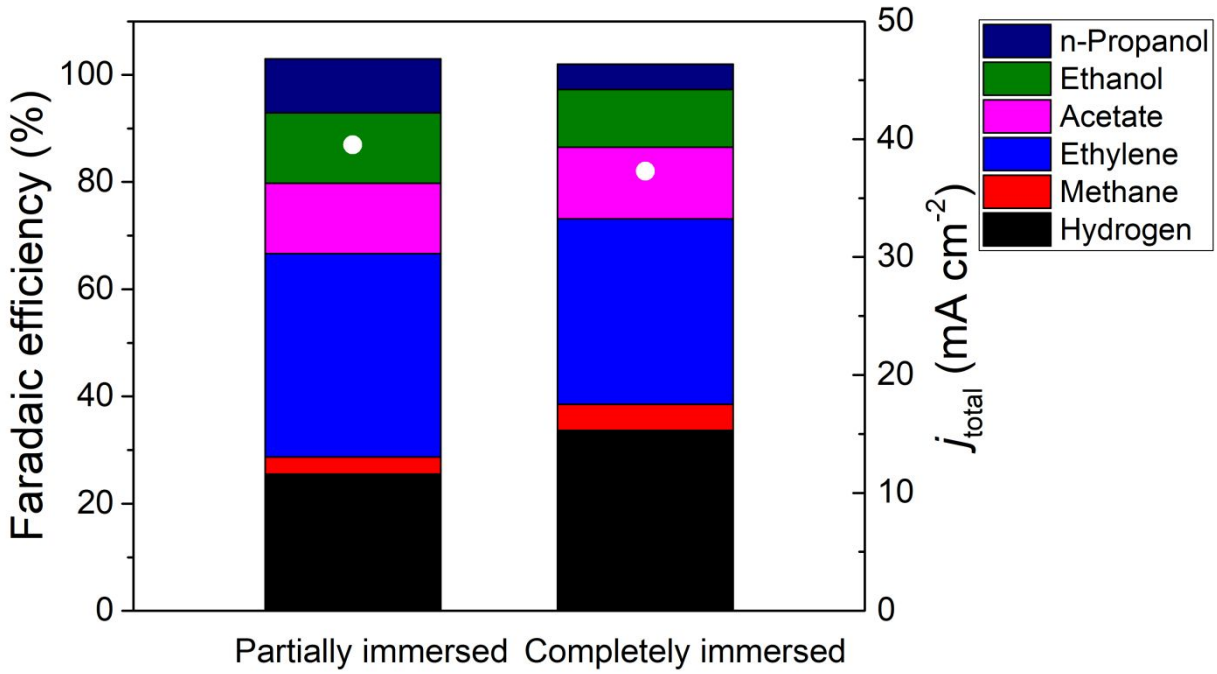

Figure S10. CO electrolysis results of a partially immersed dendritic Cu/C electrode and a completely immersed dendritic Cu/C electrode at -0.76 V. The slightly higher H_2 selectivity of the completely immersed electrode is most likely due to the presence of the nickel wire current collector and the silver epoxy in the electrolyte. This result indicates that the CO transported to the reaction sites is not from the top of the carbon fiber paper.

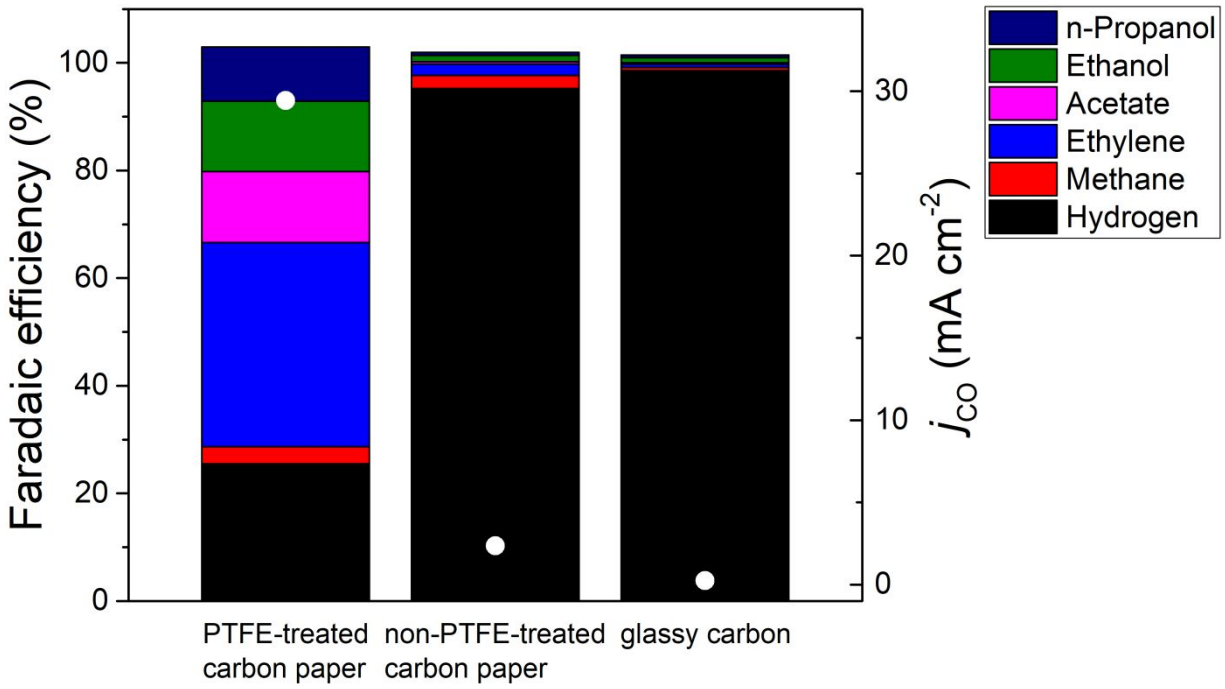

Figure S11. CO electrolysis results for different carbon support. Dendritic Cu powder catalysts were deposited on PTFE-treated carbon paper support, non-PTFE-treated carbon paper support and glassy carbon support at same mass loading. Electrodes using none-hydrophobic support exhibited significantly smaller reaction rate and Faradaic efficiency at -0.76 V.

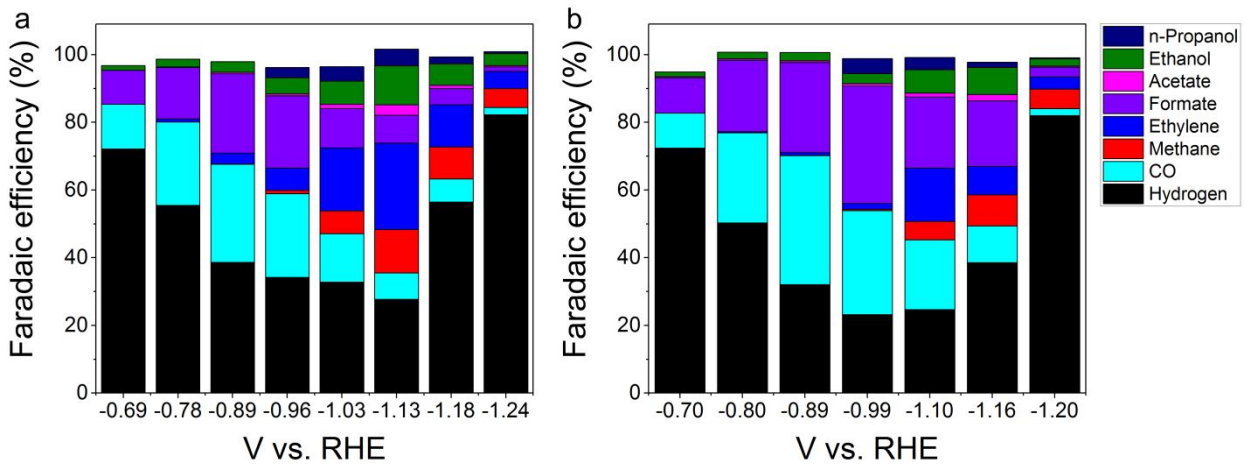

Figure S12. CO_2 electrolysis results for both Cu powders. Faradaic efficiencies of CO_2 reduction products on dendritic Cu/C electrodes (a) and spherical Cu/C electrodes (b) at different potentials.

Supplementary Methods

Predictions of the possible Tafel slopes and reaction orders of CH_4 and C_{2+} products by considering different rate-determining steps are summarized in the table below. The symmetry factor β in Tafel slope calculations is assumed to be 0.5. Detailed derivations and analysis are also presented.

Table S1. Tafel slopes and reaction orders of CH_4 formation

RDS	CO reaction order		Tafel slope	pH
	low coverage	high coverage	/ mV dec^{-1}	dependent
$*CO + *H \xrightarrow{k_{CO(H)}} *CO(H) + *$	less than 1	negative	59	yes
$*CO + H^+(aq) + e^- \xrightarrow{k_{CO(H)}} *CO(H)$	1	0	118	yes

Table S2 Tafel slopes and reaction orders of C_{2+} product formation

RDS	CO reaction order		Tafel slope	pH
	low coverage	high coverage	/ mV dec^{-1}	dependent
$*CO + *CO + e^- \xrightarrow{k_{C_2O_2^-}} *C_2O_2^- + *$	2	0	118	no
$*CO + CO(g) + e^- \xrightarrow{k_{C_2O_2^-}} *C_2O_2^-$	2	1	118	no
$*CO + *H \xrightarrow{k_{CO(H)}} *CO(H) + *$	less than 1	negative	59	yes
$*CO + H^+(aq) + e^- \xrightarrow{k_{CO(H)}} *CO(H)$	1	0	118	yes

1. Reaction order of CH_4 formation

Possibility 1

The rate-determining step (RDS) is the protonation of surface-adsorbed CO (noted as *CO). The proton source is the surface adsorbed *H.

RDS: $*CO + *H \xrightarrow{k_{CO(H)}} *CO(H) + *$

The rate of CH_4 production is determined by the coverage of *CO (θ_{CO}) and the coverage of *H (θ_H):

$$j_{CH_4} = k_{CO(H)}\theta_{CO}\theta_H \quad (1)$$

We assume a fast equilibrium for CO adsorption on the surface, where the equilibrium constant is K_{CO}:

$$CO(g) + * \xleftrightarrow{K_{CO}} *CO$$

$$K_{CO} = \frac{\theta_{CO}}{P_{CO}\theta_*} \quad (2)$$

Similarly, the reduction of H^+ to produce *H is assumed to be a fast equilibrium, and the equilibrium constant can be represented in a Nernstian-type equation:

$$H^+(aq) + e^- + * \xleftrightarrow{K_H} *H$$

$$K_H = \frac{\theta_H}{\left[H^+\right]\exp\left(\frac{\eta F}{RT}\right)\theta_*} \tag{3}$$

Because *H and *CO are the two major adsorbates, the coverage of the free adsorption site (θ_*) can be written as:

$$\theta_* \approx 1 - \theta_{CO} - \theta_H \tag{4}$$

The coverage of H_{ads} is typically considered to be small:

$$\theta_* \approx 1 - \theta_{CO} \tag{5}$$

From equations (2), (3) and (5), we can obtain:

$$\theta_{CO} = \frac{K_{CO}P_{CO}}{1 + K_{CO}P_{CO}} \tag{6}$$

$$\theta_H = \frac{K_H\left[H^+\right]\exp\left(\frac{\eta F}{RT}\right)}{1 + K_{CO}P_{CO}} \tag{7}$$

Combining equations (1), (6) and (7) yields:

$$j_{CH_4} = k_{CO(H)}\frac{K_{CO}P_{CO}K_H\left[H^+\right]\exp\left(\frac{\eta F}{RT}\right)}{(1 + K_{CO}P_{CO})^2} \tag{8}$$

According to equations (2) and (5):

$$K_{CO}P_{CO} = \frac{\theta_{CO}}{1 - \theta_{CO}} \tag{9}$$

According to equation (9), at low *CO coverage ($\theta_{CO} << 1$), the $\left(1 + K_{CO}P_{CO}\right)$ term approaches 1, and the rate expression (8) becomes:

$$j_{CH_4} = k_{CO(H)}K_H K_{CO}P_{CO}\left[H^+\right]\exp\left(\frac{\eta F}{RT}\right) \tag{10}$$

K_H is inversely correlated to P_{CO} due to the increase in the *CO coverage would reduce the coverage and binding strength of *H.[4-5] Therefore, the reaction order with respect to P_{CO} should be smaller than 1. Moreover, if the *H binding strength is significantly weakened by

a high *CO coverage, the reaction order may even become negative. This reaction scheme is consistent with the experimental observations shown in Figure 4. In addition, the concomitant substantial decrease is H_2 production is a further indication that the decrease in *H is the main cause of the negative reaction order.

At high θ_{CO}, the $\left(1+K_{CO}P_{CO}\right)$ term tends to $\left(K_{CO}P_{CO}\right)$, and the rate expression becomes:

$$j_{CH_4} = k_{CO(H)}K_H\left[H^+\right]\exp\left(\frac{\eta F}{RT}\right)\frac{1}{K_{CO}P_{CO}} \tag{11}$$

The reaction order with respect to P_{CO} is less than -1 for the same reason as that in equation (10).

This reaction scheme can be consistent with the experimental observations shown in Figure 4.

Possibility 2

The RDS is the protonation of *CO. The hydrogen source is the proton (or water) in the electrolyte.

RDS: $*CO + H^+(aq) + e^- \xrightarrow{k_{CO(H)}} *CO(H)$

The rate expression can be written as:

$$j_{CH_4} = k_{CO(H)}\theta_{CO}\left[H^+\right]\exp\left(\frac{\beta\eta F}{RT}\right) \tag{12}$$

where β is the symmetry factor for the reduction process.

We assume a fast equilibrium for CO adsorption on the surface, where the equilibrium constant is: K_{CO}:

$CO(g) + * \xleftarrow{K_{CO}} *CO$

$$K_{CO} = \frac{\theta_{CO}}{P_{CO}\theta_*} \tag{13}$$

Because *CO is the only major adsorbate, θ_* can be expressed as:

$$\theta_* \approx 1 - \theta_{CO} \tag{14}$$

From equations (13) and (14), we can obtain:

$$\theta_{CO} = \frac{K_{CO}P_{CO}}{1+K_{CO}P_{CO}} \tag{15}$$

Combining equations (12) and (15) yields:

$$j_{CH_4} = k_{CO(H)}\left[H^+\right]\exp\left(\frac{\beta\eta F}{RT}\right)\frac{K_{CO}P_{CO}}{1+K_{CO}P_{CO}} \quad (16)$$

According to equations (13) and (14):

$$K_{CO}P_{CO} = \frac{\theta_{CO}}{1-\theta_{CO}} \quad (17)$$

At low *CO coverage ($\theta_{CO} << 1$), according to equation (17), the $\left(1+P_{CO}K_{CO}\right)$ term approaches 1, and the rate expression (16) becomes:

$$j_{CH_4} = k_{CO(H)}\left[H^+\right]\exp\left(\frac{\beta\eta F}{RT}\right)K_{CO}P_{CO} \quad (18)$$

The reaction order with respect to P_{CO} is 1.

At high θ_{CO}, the $\left(1+K_{CO}P_{CO}\right)$ term tends to $\left(K_{CO}P_{CO}\right)$, and the rate expression can be expressed as:

$$j_{CH_4} = k_{CO(H)}\left[H^+\right]\exp\left(\frac{\beta\eta F}{RT}\right) \quad (19)$$

The reaction order with respect to P_{CO} is 0.

This reaction scheme is not consistent with the experimental observations shown in Figure 4.

2. Reaction order of C_{2+} Production

a. Dimerization between two *CO

The RDS is the coupling between two *CO.

RDS: $*CO + *CO + e^- \xrightarrow{k_{C_2O_2^-}} *C_2O_2^- + *$

The rate expression can be written as:

$$j_{C_{2+}} = k_{C_2O_2^-}\theta_{CO}{}^2\exp\left(\frac{\beta\eta F}{RT}\right) \quad (20)$$

We assume a fast equilibrium for CO adsorption on the surface, where the equilibrium constant is K_{CO}:

$$CO(g) + * \xleftrightarrow{K_{CO}} *CO$$

$$K_{CO} = \frac{\theta_{CO}}{P_{CO}\theta_*} \quad (21)$$

Because *CO is the only major adsorbate, θ_* can be expressed as:

$$\theta_* \approx 1-\theta_{CO} \tag{22}$$

From equations (21) and (22), we can obtain:

$$\theta_{CO} = \frac{K_{CO}P_{CO}}{1+K_{CO}P_{CO}} \tag{23}$$

Combining equations (20) and (23) yields:

$$j_{C_{2+}} = k_{C_2O_2^-} \exp\left(\frac{\beta\eta F}{RT}\right)\left(\frac{K_{CO}P_{CO}}{1+K_{CO}P_{CO}}\right)^2 \tag{24}$$

According to equations (21) and (22):

$$K_{CO}P_{CO} = \frac{\theta_{CO}}{1-\theta_{CO}} \tag{25}$$

At low *CO coverage ($\theta_{CO} << 1$), according to equation (25), the $\left(1+K_{CO}P_{CO}\right)$ term approaches 1, and the rate expression (24) can be expressed as:

$$j_{C_{2+}} = k_{C_2O_2^-} \exp\left(\frac{\beta\eta F}{RT}\right) K_{CO}{}^2 P_{CO}{}^2 \tag{26}$$

The reaction order with respect to P_{CO} is 2.

At high θ_{CO}, the $\left(1+K_{CO}P_{CO}\right)$ term tends to $\left(K_{CO}P_{CO}\right)$, and the rate expression becomes:

$$j_{C_{2+}} = k_{C_2O_2^-} \exp\left(\frac{\beta\eta F}{RT}\right) \tag{27}$$

The reaction order with respect to P_{CO} is 0.

This reaction scheme can be consistent with the experimental observations shown in Figure 4.

b. Dimerization between *CO and CO

The RDS is the coupling between *CO and a CO molecule:

RDS: $*CO + CO(g) + e^- \xrightarrow{k_{C_2O_2^-}} *C_2O_2^-$

The rate expression can be written as:

$$j_{C_{2+}} = k_{C_2O_2^-}\theta_{CO}P_{CO}\exp\left(\frac{\beta\eta F}{RT}\right) \quad (28)$$

We assume a fast equilibrium for CO adsorption on the surface, where the equilibrium constant is K_{CO}:

$$CO(g) + * \xleftrightarrow{K_{CO}} *CO$$

$$K_{CO} = \frac{\theta_{CO}}{P_{CO}\theta_*} \quad (29)$$

Because *CO is the only major adsorbate, θ_* can be expressed as:

$$\theta_* \approx 1 - \theta_{CO} \quad (30)$$

From equations (29) and (30), we can obtain:

$$\theta_{CO} = \frac{K_{CO}P_{CO}}{1 + K_{CO}P_{CO}} \quad (31)$$

Combining equations (28) and (31) yields:

$$j_{C_{2+}} = k_{C_2O_2^-}\exp\left(\frac{\beta\eta F}{RT}\right)\frac{K_{CO}P_{CO}^{\ 2}}{1 + K_{CO}P_{CO}} \quad (32)$$

According to equations (29) and (30):

$$K_{CO}P_{CO} = \frac{\theta_{CO}}{1 - \theta_{CO}} \quad (33)$$

At low *CO coverage ($\theta_{CO} << 1$), according to equation (33), the $\left(1 + K_{CO}P_{CO}\right)$ term approaches 1, and the rate expression (32) can be expressed as:

$$j_{C_{2+}} = k_{C_2O_2^-}\exp\left(\frac{\beta\eta F}{RT}\right)K_{CO}P_{CO}^{\ 2} \quad (34)$$

The reaction order for P_{CO} is 2.

At high θ_{CO}, the $\left(1 + K_{CO}P_{CO}\right)$ term approaches $\left(K_{CO}P_{CO}\right)$, and the rate expression becomes:

$$j_{C_{2+}} = k_{C_2O_2^-}\exp\left(\frac{\beta\eta F}{RT}\right)P_{CO} \quad (35)$$

The reaction order with respect to P_{CO} is 1.

This reaction scheme is not consistent with the experimental observations shown in Figure 4.

c. Dimerization between *CO(H) and *CO (or CO)

Possibility 1

The RDS is the protonation of *CO. The proton source is *H. C_{2+} is produced via C-C coupling between CO and the product of *CO hydrogenation (noted as *CO(H)).

RDS: $*CO + *H \xrightarrow{k_{CO(H)}} *CO(H) + *$

C_{2+} production: $*CO$ (or $CO(g)$) $+ *CO(H) \xrightarrow{k_{C_2O_2(H)}} *C_2O_2$(H)+*

The rate expression can be written as:

$$j_{C_{2+}} = k_{C_2O_2(H)}\theta_{CO}\theta_{CO(H)} \text{ (or } = k_{C_2O_2(H)}P_{CO}\theta_{CO(H)}) = k_{CO(H)}\theta_{CO}\theta_H \quad (36)$$

We assume a fast equilibrium for both CO and H adsorption on the surface, where the equilibrium constants are K_{CO} and K_H, respectively:

$$CO(g) + * \xleftrightarrow{K_{CO}} *CO$$

$$K_{CO} = \frac{\theta_{CO}}{P_{CO}\theta_*} \quad (37)$$

$$H^+(aq) + e^- + * \xleftrightarrow{K_H} *H$$

$$K_H = \frac{\theta_H}{\left[H^+\right]\exp\left(\frac{\eta F}{RT}\right)\theta_*} \quad (38)$$

The H_{ads} coverage is typically considered to be small. $\theta_{CO(H)}$ is also small due to its consumption being faster than its production. Therefore, *CO is the only major adsorbate, and θ_* can be expressed as:

$$\theta_* \approx 1 - \theta_{CO} \quad (39)$$

From equations (37), (38) and (39), we can obtain:

$$\theta_{CO} = \frac{K_{CO}P_{CO}}{1 + K_{CO}P_{CO}} \quad (40)$$

$$\theta_H = \frac{K_H\left[H^+\right]\exp\left(\frac{\eta F}{RT}\right)}{1 + K_{CO}P_{CO}} \quad (41)$$

Combining equations (36), (40) and (41) yields:

$$j_{C_{2+}} = k_{CO(H)} \frac{K_{CO} P_{CO} K_H \left[H^+\right] \exp\left(\frac{\eta F}{RT}\right)}{\left(1 + K_{CO} P_{CO}\right)^2} \quad (42)$$

According to equations (37) and (39):

$$K_{CO} P_{CO} = \frac{\theta_{CO}}{1 - \theta_{CO}} \quad (43)$$

At low *CO coverage ($\theta_{CO} << 1$), according to equation (43), the $\left(1 + K_{CO} P_{CO}\right)$ term approaches 1, and the rate expression (42) can be expressed as:

$$j_{C_{2+}} = k_{CO(H)} K_{CO} P_{CO} K_H \left[H^+\right] \exp\left(\frac{\eta F}{RT}\right) \quad (44)$$

The reaction order with respect to P_{CO} is smaller than 1 for the same reason as that in equation (10).

At high θ_{CO}, the $\left(1 + K_{CO} P_{CO}\right)$ term approaches $\left(K_{CO} P_{CO}\right)$, and the rate expression becomes:

$$j_{C_{2+}} = k_{CO(H)} K_H \left[H^+\right] \exp\left(\frac{\eta F}{RT}\right) \frac{1}{K_{CO} P_{CO}} \quad (45)$$

The reaction order with respect to P_{CO} is smaller than -1 for the same reason as that in equation (11).

This reaction scheme is not consistent with the experimental observations shown in Figure 4.

Possibility 2

The RDS is the hydrogenation of surface-bound CO (noted as *CO). The hydrogen source is the proton (or water) in solution. C_{2+} is produced via CO coupling between CO and *CO(H).

RDS: $*CO + H^+(aq) + e^- \xrightarrow{k_{CO(H)}} *CO(H)$

C_{2+} production: $*CO$ (or $CO(g)$) $+ *CO(H) \xrightarrow{k_{C_2O_2(H)}} *C_2O_2$(H)+*

The rate expression can be written as:

$$j_{C_{2+}} = k_{C_2O_2(H)} \theta_{CO} \theta_{CO(H)} \text{ (or } = k_{C_2O_2(H)} P_{CO} \theta_{CO(H)}) = k_{CO(H)} \theta_{CO} \left[H^+\right] \exp\left(\frac{\beta \eta F}{RT}\right) \quad (46)$$

We assume a fast equilibrium for CO adsorption on the surface, where the equilibrium constant is K_{CO}:

$$CO(g) + * \xleftrightarrow{K_{CO}} *CO$$

$$K_{CO} = \frac{\theta_{CO}}{P_{CO}\theta_*} \tag{47}$$

$\theta_{CO(H)}$ is small due to its consumption being faster than its production. Therefore, *CO is the only major adsorbate, and θ_* can be expressed as:

$$\theta_* \approx 1 - \theta_{CO} \tag{48}$$

From equations (47) and (48), we can obtain:

$$\theta_{CO} = \frac{K_{CO}P_{CO}}{1 + K_{CO}P_{CO}} \tag{49}$$

Combining equations (46) and (49) yields:

$$j_{C_{2+}} = k_{CO(H)} \frac{K_{CO}P_{CO}\left[H^+\right]\exp\left(\frac{\beta\eta F}{RT}\right)}{1 + K_{CO}P_{CO}} \tag{50}$$

According to equations (47) and (48):

$$K_{CO}P_{CO} = \frac{\theta_{CO}}{1 - \theta_{CO}} \tag{51}$$

At low *CO coverage ($\theta_{CO} << 1$), according to equation (51), the $\left(1 + K_{CO}P_{CO}\right)$ term approaches 1, and the rate expression (50) can be expressed as:

$$j_{C_{2+}} = k_{CO(H)}K_{CO}P_{CO}\left[H^+\right]\exp\left(\frac{\beta\eta F}{RT}\right) \tag{52}$$

The reaction order with respect to P_{CO} is 1.

At high θ_{CO}, the $\left(1 + K_{CO}P_{CO}\right)$ term approaches $\left(K_{CO}P_{CO}\right)$, and the rate expression becomes:

$$j_{C_{2+}} = k_{CO(H)}K_{CO}\left[H^+\right]\exp\left(\frac{\beta\eta F}{RT}\right) \tag{53}$$

The reaction order with respect to P_{CO} is 0.

This reaction scheme can be consistent with the experimental observations shown in Figure 4. However, it leads to a pH dependence of C_{2+} products formation which is apparently against the current understanding that C_2H_4 formation is pH independent.

Supplementary Reference

1. Platzman, I.; Brener, R.; Haick, H.; Tannenbaum, R. Oxidation of Polycrystalline Copper Thin Films at Ambient Conditions. *J. Phys. Chem. C* **2008,** 112, 1101-1108.
2. Dubot, P.; Jousset, D.; Pinet, V.; Pellerin, F.; Langeron, J. P. Simulation of the Lmm Auger-Spectra of Copper. *Surf. Interface Anal.* **1988,** 12, 99-104.
3. Poulston, S.; Parlett, P. M.; Stone, P.; Bowker, M. Surface Oxidation and Reduction of CuO and Cu2O Studied Using XPS and XAES. *Surf. Interface Anal.* **1996,** 24, 811-820.
4. Zhang, Y.-J.; Sethuraman, V.; Michalsky, R.; Peterson, A. A. Competition between CO2 Reduction and H2 Evolution on Transition-Metal Electrocatalysts. *ACS Catal.* **2014,** 4, 3742-3748.
5. Schreier, M.; Yoon, Y.; Jackson, M. N.; Surendranath, Y. Competition between H and CO for Active Sites Governs Copper-Mediated Electrosynthesis of Hydrocarbon Fuels. *Angew. Chem., Int. Ed.* **2018,** 57, 10221-10225.